ACS Catalysis

Research Article

pubs.acs.org/acscatalysis

HheG, a Halohydrin Dehalogenase with Activity on Cyclic Epoxides

Julia Koopmeiners,[†,§] Christina Diederich,[‡,∥] Jennifer Solarczek,[†] Hauke Voß,[†] Janine Mayer,[†] Wulf Blankenfeldt,[†,‡] and Anett Schallmey*[,†]

[†]Institute for Biochemistry, Biotechnology and Bioinformatics, Technische Universität Braunschweig, Spielmannstraße 7, 38106 Braunschweig, Germany

[‡]Structure and Function of Proteins, Helmholtz Centre for Infection Research, Inhoffenstraße 7, 38124 Braunschweig, Germany

Supporting Information

ABSTRACT: Halohydrin dehalogenases (HHDHs) are of biotechnological interest due to their promiscuous epoxide ring-opening activity with a set of negatively charged nucleophiles, enabling the formation of C−C, C−N, or C−O bonds. The recent discovery of HHDH-specific sequence motifs aided the identification of a large number of halohydrin dehalogenases from public sequence databases, enlarging the biocatalytic toolbox substantially. During the characterization of 17 representatives of these phylogenetically diverse enzymes, one HHDH, namely HheG from *Ilumatobacter coccineus*, was identified to convert cyclic epoxide substrates. The enzyme exhibits significant activity in the azidolysis of cyclohexene oxide and limonene oxide with turnover numbers of 7.8 and 44 s^{-1}, respectively. As observed for other HHDHs, the cyanide-mediated epoxide ring-opening proceeded with lower rates. Wild-type HheG displays modest enantioselectivity, as the resulting azido- and cyanoalcohols of cyclohexene oxide ring-opening were obtained in 40% enantiomeric excess. These biocatalytic findings were further complemented by the crystal structure of the enzyme refined to 2.3 Å. Analysis of HheG's structure revealed a large open cleft harboring the active site. This is in sharp contrast to other known HHDH structures and aids in explaining the special substrate scope of HheG.

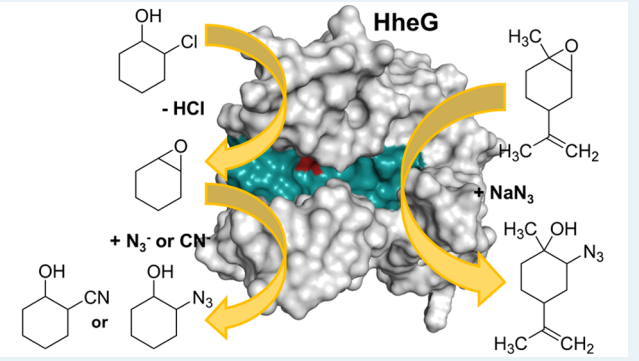

KEYWORDS: *halohydrin dehalogenase, epoxide ring-opening, cyclohexene oxide, limonene oxide, biotransformation, crystal structure*

INTRODUCTION

Halohydrin dehalogenases (HHDHs; also called haloalcohol dehalogenases or epoxidases) are biocatalytically attractive enzymes for the synthesis of various β-substituted alcohols due to their promiscuous epoxide ring-opening activity with a range of anionic nucleophiles such as azide, cyanide, nitrite, cyanate, and formate.[1] As their natural reaction, they catalyze the reversible dehalogenation of vicinal haloalcohols with formation of the corresponding epoxides. Since their discovery in 1968,[2] many different biotechnological applications of HHDHs have been described on the basis of merely a handful of known HHDH enzymes. One of the most prominent examples is their use in the synthesis of ethyl (*R*)-4-cyano-3-hydroxybutyrate, a chiral synthon for the production of statin side chains.[3] This process has been applied on the industrial scale, employing a stereoselective ketoreductase in combination with a highly engineered variant of HheC from *Agrobacterium tumefaciens* AD1.[4] The putative process variant of HheC carries a minimum of 35 amino acid exchanges which had been generated by ProSAR-driven enzyme evolution to significantly improve the volumetric productivity of the HHDH-catalyzed step.[4] Other examples for biocatalytic applications of HHDHs include the synthesis of chiral C3 units, such as epihalohydrins,[5] as well as the synthesis of highly enantioenriched oxazolidinones[6,7] and tertiary alcohols.[8,9]

HHDHs belong to the superfamily of short-chain dehydrogenases/reductases (SDR), with which they share considerable sequence homology as well as structural and mechanistic features.[10] Recently, HHDH-specific sequence motifs have been described that enable the unambiguous discrimination of HHDH sequences from the overwhelming majority of SDR enzymes.[11] Using a database mining approach based on these motifs, the number of HHDH sequences could be increased by at least 10-fold. Until 2016, 69 diverse HHDH enzyme sequences have been reported that can be subdivided into six phylogenetic subtypes with sequence identities below 30%.[1] A selection of 17 new HHDHs, representing all phylogenetic subtypes, has been characterized in more detail.[12] Interestingly, five of the tested enzymes displayed higher thermostabilities and temperature optima in comparison to the well-known HheC.

Until now, HHDHs have been described to convert only terminal epoxides, resulting in a highly regioselective attack of

Received: June 7, 2017
Revised: August 24, 2017

© XXXX American Chemical Society

DOI: 10.1021/acscatal.7b01854
ACS Catal. 2017, 7, 6877−6886

the nucleophile at the sterically less hindered β-carbon atom. In a study by Elenkov et al., vicinally disubstituted as well as cyclic epoxides have been tested in reactions with HheC in addition to HheA2 from *Arthrobacter* sp. AD2 and HheB2 from *Mycobacterium* sp. GP1.[13] None of the enzymes used, however, were able to convert these sterically more demanding epoxide substrates. With our large set of highly diverse new HHDHs at hand, we anticipated that it should be possible to identify enzymes with novel catalytic features. In particular, the selective epoxide ring-opening of cyclic epoxides using HHDHs would be of high interest, as this would enable access to chiral synthons for the production of pharmaceuticals such as (1*R*,2*S*)-4-((2-cyanocyclohexyl)oxy)-2-(trifluoromethyl)-benzonitrile, a potent androgen receptor antagonist.[14]

RESULTS AND DISCUSSION

Conversion of Cyclic Epoxides by HHDHs. To investigate the activity of new HHDHs toward cyclic epoxides, our 17 previously characterized HHDHs[12] together with the well-known HheC from *A. tumefaciens*[10] were applied in conversions of cyclohexene oxide (**2**) and (+)-*cis*/(+)-*trans*-limonene oxide (**5**). Reactions were carried out using sodium azide as the nucleophile to yield azido alcohols **4** and **6**, respectively, as products (Scheme 1). One enzyme, HheG from

Scheme 1. Substrates and Products of Cascade and Epoxide Ring-Opening Reactions[a]

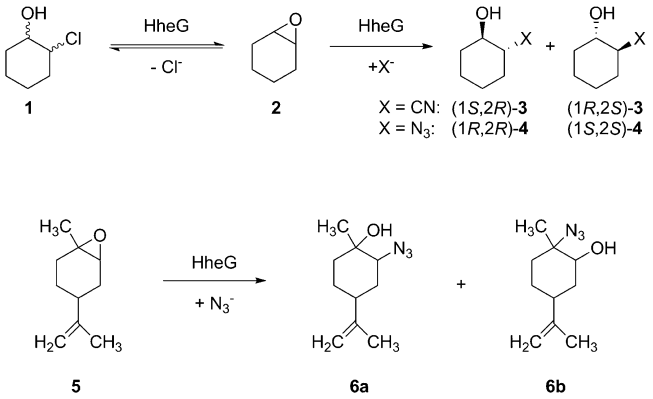

[a]Substrates: 2-chlorocyclohexanol (**1**), cyclohexene oxide (**2**), limonene oxide (**5**); products: 2-cyano-1-cyclohexanol (**3**); 2-azido-1-cyclohexanol (**4**); 2-azido-1-methyl-4-(prop-1-en-2-yl)cyclohexan-1-ol (**6a**), and 2-azido-2-methyl-5-(prop-1-en-2-yl)cyclohexan-1-ol (**6b**).

Ilumatobacter coccineus, catalyzed the complete conversion of cyclic epoxide **2**, yielding 2-azido-1-cyclohexanol (**4**) as the product (Figure 1). All other tested HHDHs, including the previously described HheC, showed only low conversion (up to 40%). Considering that the chemical background azidolysis already yielded up to 30% of **4**, only HheG showed a significant enzymatic activity on **2**. Interestingly, in previous studies on the substrate scope of HheG, only low specific activities were obtained toward aliphatic haloalcohols such as 1,3-dichloro-2-propanol (<0.1 U mg^{-1}) and ethyl 4-chloro-3-hydroxybutyrate (0.2 U mg^{-1}) as well as the arylaliphatic haloalcohol 2-chloro-1-phenylalcohol (<0.1 U mg^{-1}).[12] The corresponding epoxides, epichlorohydrin and styrene oxide, were also hardly converted with azide as nucleophile. The only HheG substrate for which a high activity has been reported so far is epoxide glycidylphenyl ether, for which a product yield of 100% was achieved in the azidolysis reaction. Similarly, HheG also achieved the highest product yields (98% after 24 h) in the azidolysis of **5** in comparison to other HHDHs (Figure 1). Only HheE5 (62% conversion) and HheF (79% conversion) also exhibited significant activity on **5** in comparison to the chemical background reaction giving 15% of **6**. To the best of our knowledge, HheG therefore is the first HHDH reported to accept cyclic epoxide substrates in epoxide ring-opening reactions.

Kinetic Characterization of HheG. In order to investigate HheG's ability to convert cyclic substrates in more detail, kinetic parameters of HheG in the conversion of epoxides **2** and **5** with azide and cyanide were determined. In addition, HheG kinetics in the dehalogenation of chlorocyclohexanol (**1**) were measured (Table 1). Since fitting of the obtained experimental data to the Michaelis–Menten equation was poor, the Hill equation was used instead. Comparison of the obtained kinetic constants for the three tested substrates (**1**, **2**, and **5**) revealed significant differences. The highest K_{50} value (30 mM) was observed for haloalcohol **1**, whereas the K_{50} value for the corresponding epoxide **2** was lower. Furthermore, HheG's turnover number (k_{cat}) in the azidolysis of **2** was more than 20 times higher than the dehalogenation of the corresponding chloroalcohol **1**. Moreover, azidolysis of **5** with a k_{cat} value of 44 s^{-1} was about 5.5 times faster than the azidolysis of epoxide **2** (k_{cat} value of 7.8 s^{-1}). Interestingly, the Hill coefficient for the azidolysis of **5** (n_H = 1.7) by HheG is lower than that for azidolysis of **2** (n_H = 3). This suggests a stronger cooperativity for binding of epoxide **2** to HheG than for binding of epoxide **5**. A comparison of the obtained K_{50} values for the nucleophiles azide (8.6 mM) and cyanide (20 mM) indicates a higher affinity of HheG toward azide. Similarly, HheG displayed a stronger cooperativity for binding of CN^- (n_H = 3.3) than for N_3^- (n_H = 1.7). This might explain why the determined k_{cat} value in the cyanolysis of **2** was more than 1000-fold lower than that in the respective azidolysis reaction. For azide a fixed nucleophile concentration of 50 mM was used, while the nucleophile concentration was set to 75 mM for cyanide. Especially in the case of cyanide, this nucleophile concentration might not have been high enough to exclude any major influence on the kinetic experiments. For cyanide, however, higher nucleophile concentrations lead to substantial nonenzymatic product formation observed as high chemical background. The dependence of HHDH activity in the epoxide ring-opening reactions on the type of nucleophile is well in line with previous observations.[15] When nine different nucleophiles were tested in the epoxide ring-opening of epoxybutane using HheC, a 64-fold higher k_{cat} value was observed when azide was used as the nucleophile in comparison to cyanide. Moreover, of all nine tested nucleophiles HheC exhibited the highest activity with azide.

Interestingly, this is the first report for cooperative substrate binding to a HHDH. Previous kinetic analysis of several other HHDHs has not provided evidence for cooperative behavior of these enzymes.[7,10,16] The Hill coefficients reported here may therefore indicate that HheG varies from other HHDHs by requiring structural changes across the homotetramer in the course of the catalytic cycle.

In a previous report, it was observed that HheG is quite thermolabile, exhibiting a T_{50}^{10} value (half inactivation temperature after incubation for 10 min) of 40 °C.[12] In these initial stability experiments, however, residual activity was determined on the basis of substrate dehalogenation. Given that HheG is

DOI: 10.1021/acscatal.7b01854
ACS Catal. 2017, 7, 6877–6886

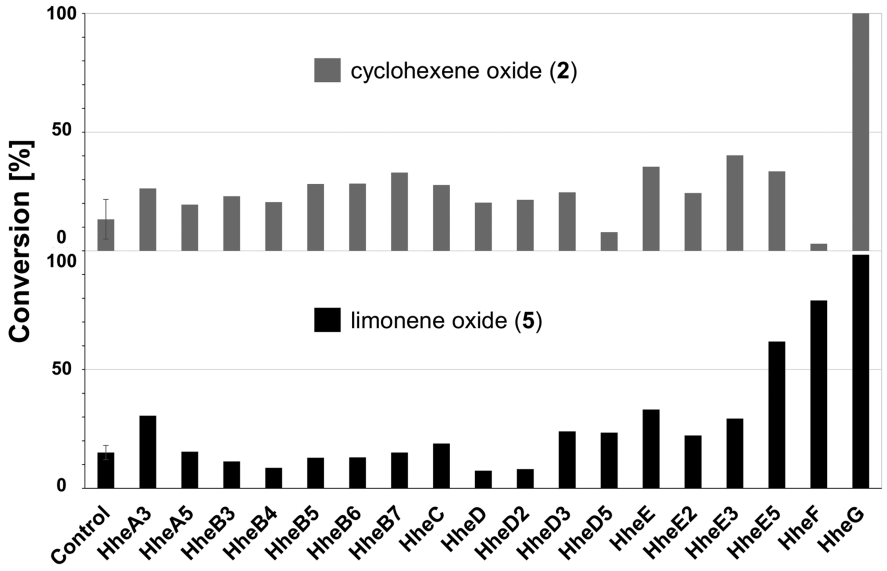

Figure 1. Conversions obtained in reactions of cyclohexene oxide (**2**) and (+)-*cis*/(+)-*trans*-limonene oxide (**5**) using purified HHDH and azide as nucleophile. Control reactions were carried out in buffer without enzymes.

Table 1. Kinetic Parameters of HheG with Substrates Chlorocyclohexanol (1), Cyclohexene Oxide (2), and (+)-*cis*-/(+)-*trans*-Limonene Oxide (5) Using Cyanide (NaCN) or Azide (NaN_3) as Nucleophile, as well as K_{50} Values of Nucleophiles Azide and Cyanide

	K_{50} (mM)	k_{cat} (s^{-1})	k_{cat}/K_{50} (mM^{-1} s^{-1})	n_H
chlorocyclohexanol (**1**)	30.0 ± 3.0	0.3 ± 0.03	0.01 ± 0.01	2.9 ± 0.6
cyclohexene oxide (**2**) [NaCN]	22.2 ± 2.0	(2 ± 0.00) × 10^{-4}	(7.7 ± 0.00) × 10^{-6}	2.6 ± 0.5
cyclohexene oxide (**2**) [NaN_3]	23.7 ± 2.6	7.8 ± 0.35	0.3 ± 0.13	3.0 ± 0.9
(+)-*cis*-/(+)-*trans*-limonene oxide (**5**) [NaN_3]	19.4 ± 2.4	44 ± 0.01	2.3 ± 0.00	1.7 ± 0.3
NaN_3 [cyclohexene oxide]	8.6 ± 0.5			1.7 ± 0.2
NaCN [cyclohexene oxide]	19.8 ± 0.5			3.3 ± 0.3

more active in the epoxide ring-opening of cyclic epoxides, temperature and pH optima of HheG were determined in the epoxide ring-opening of **2** using N_3^- as nucleophile here (Figure S1 in the Supporting Information). This gave a temperature optimum of 30 °C and a complete enzyme inactivation at 40 °C, confirming that HheG is quite unstable. The obtained pH optimum between pH 6 and 7 is in the range of previously studied HHDHs with HheA, HheB, and HheC, showing an optimum in the epoxide ring-opening between pH 4 and 7.[10,17−20]

Stereoselectivity of HheG. Cyanolysis of **2** leads to the production of *trans*-2-hydroxycyclohexane-1-carbonitrile (**3**). The 1*S*,2*R* enantiomer of this compound serves as an intermediate in the synthesis of the androgen receptor antagonist (1*R*,2*S*)-4-((2-cyanocyclohexyl)oxy)-2-(trifluoromethyl)benzonitrile[21] and is therefore of industrial interest. To analyze HheG's selectivity in the cyanolysis of **2**, reactions with purified HheG, 5 mM **2**, and 20 mM NaCN were carried out at room temperature and analyzed by chiral GC after extraction. A moderate enantiomeric excess (ee) of cyanoalcohol **3** with 37% ee after 30 min reaction time was obtained. The enantiomeric excess slightly decreased upon prolonged incubation due to a significant chemical background cyanolysis reaction. Using chiral GC and a lipase-catalyzed enantiomeric separation strategy,[22,23] the stereoconfiguration of the preferentially formed enantiomer was determined and confirmed that HheG favors the formation of (1*S*,2*R*)-**3** (Scheme 1). Thus, HheG's enantiopreference opens a new biocatalytic route toward the androgen receptor antagonist (1*R*,2*S*)-4-((2-cyanocyclohexyl)oxy)-2-(trifluoromethyl)-benzonitrile.[14]

In the azidolysis of **2**, HheG exhibited an ee value of 40% for the formation of one enantiomer of azidoalcohol **4**. To determine the stereoconfiguration of this enantiomer, azidoalcohol **4** was chemically reduced to the corresponding aminoalcohol and further analyzed by chiral GC after derivatization. By comparison with enantiopure authentic standards of (1*R*,2*R*)- and (1*S*,2*S*)-2-aminocyclohexan-1-ol, it was observed that HheG favors the formation of (1*S*,2*S*)-**4** (Scheme 1). Interestingly, this is the opposite enantiomer in comparison to the preferentially formed 1*S*,2*R* enantiomer of cyanoalcohol **3**.

Whole-Cell Biotransformation of Cyclohexene Oxide and Cascade Reaction. Production of cyanoalcohol **3** and azidoalcohol **4** was also tested using HheG-overexpressing *E. coli* cells at OD_{600} = 40. In addition, we extended our investigation to the cascade-type reaction starting from chloroalcohol **1** (Scheme 1). This strategy of combining dehalogenation and epoxide ring-opening in a cascade-type reaction using HHDHs was previously reported for the conversion of ethyl 4-chloro-3-hydroxybutyrate into ethyl 4-cyano-3-hydroxybutyrate.[4] With 20 mM chloroalcohol **1** as the starting material, the whole-cell system efficiently catalyzed the formation of epoxide **2** as intermediate as well as subsequent epoxide ring-opening due to the presence of 40 mM NaCN in the reaction mixture. After 24 h, cyanoalcohol **3** was obtained

DOI: 10.1021/acscatal.7b01854
ACS Catal. 2017, 7, 6877−6886

with a yield of 50%. After that, the product yield increased only slightly, indicating an inactivation of the whole-cell catalyst (Figure 2A). Interestingly, the chemical background cyanolysis

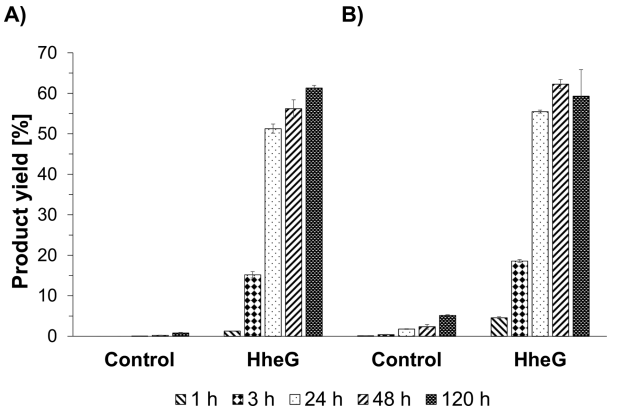

Figure 2. Product yields of whole-cell biotransformations: comparison of (A) cascade reaction starting from haloalcohol **1** (20 mM) to cyanoalcohol **3** and (B) epoxide ring-opening of **2** (20 mM) to product **3** using HheG expressing *E. coli* BL21(DE3) cells (OD_{600} = 40) and 40 mM sodium cyanide (NaCN). Control reactions were performed using the same reaction conditions with whole cells of *E. coli* BL21(DE3) lacking HheG. Error bars represent standard deviations of duplicate measurements.

of **2** in the cascade reaction was very low (<5% after 120 h) despite the high nucleophile load. This reduced chemical background had a beneficial effect on the ee value of **3**, as in the cascade reaction (1*S*,2*R*)-**3** was obtained with 40% ee. When the cascade reaction was compared to the epoxide ring-opening of **2** using whole cells, it was striking that in both cases similar yields (around 60%) of cyanoalcohol **3** were obtained (Figure 2B). The chemical background cyanolysis of **2**, however, was significantly higher when epoxide **2** was used as the starting substrate and caused a slight drop in ee value of **3** to 36%. In further tests with increased substrate and nucleophile loads (50 and 100 mM, respectively), the product yield of **3** could be increased to roughly 80%. A higher nucleophile concentration, on the other hand, led to a higher unselective chemical background, resulting in a drop in ee value for **3** of below 30%. In future applications, cyanide could be titrated to the reaction mixture as reported previously for the synthesis of ethyl (*R*)-3-hydroxyglutarate by combination of an HHDH and a nitrilase.[24] This way, the nucleophile concentration can be kept at a value that enables sufficient HHDH cyanolysis activity and at the same time limits the chemical background reaction to ensure maximum product enantiomeric excess.

The whole-cell cascade setup was also successfully applied in reactions producing azidoalcohol **4** from chloroalcohol **1**. Here, 100% yield with low chemical background (<5%) and an ee value for product **4** of 40% were obtained after 24 h.

Biotransformation of Limonene Oxide and Product Analysis. Azidolysis of (+)-*cis*-/(+)-*trans*-**5** to produce azidoalcohol **6** was also carried out using *E. coli* whole cells overexpressing HheG (Figure 3). Production of **6** using whole cells was very fast and yielded 80% conversion already after 1 h incubation at room temperature. Due to the fast conversion, the chemical background remained low. Azide-mediated epoxide ring-opening of **5** could lead to the formation of two possible regioisomers, namely 2-azido-1-methyl-4-(prop-1-en-2-yl)-cyclohexan-1-ol (**6a**) and 2-azido-2-methyl-5-(prop-1-en-2-yl)-

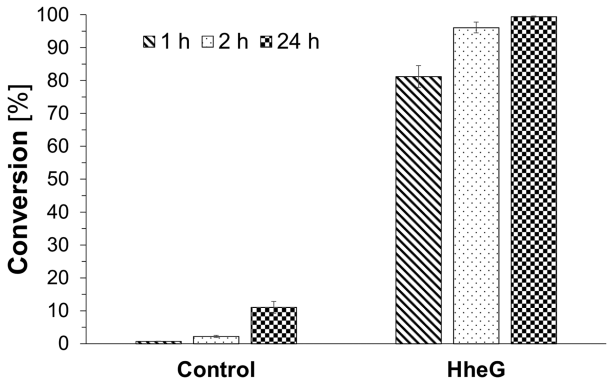

Figure 3. Azidolysis of (+)-*cis*-/(+)-*trans*-limonene oxide (**5**) to azidoalcohol **6** using 20 mM **5**, 40 mM NaN_3, and whole cells of *E. coli* BL21(DE3) overexpressing HheG with an OD_{600} value of 40. Control reactions contained *E. coli* BL21(DE3) cells carrying empty vector pET-28a. Error bars represent standard deviations of duplicate measurements.

cyclohexan-1-ol (**6b**), depending on the carbon atom that is attacked by the nucleophile (Scheme 1). Due to the lack of commercial standards for azidoalcohols **6a,b**, the azidolysis reaction of (+)-*trans*-limonene oxide ((+)-*trans*-**5**) using whole cells was scaled up for subsequent product isolation. On the basis of NMR analysis of purified product **6**, HheG converts (+)-*trans*-**5** exclusively into (+)-*trans*-2-azido-1-methyl-4-(prop-1-en-2-yl)cylohexan-1-ol ((+)-*trans*-**6a**). Hence, the nucleophile exclusively attacked the sterically less hindered carbon atom of the epoxide ring, resulting in formation of a tertiary alcohol with absolute regioselectivity. This regioselectivity is in line with the reported selectivity of previously characterized HHDHs in the epoxide ring-opening of 2,2-disubstituted terminal epoxides also yielding the corresponding tertiary alcohols exclusively.[13]

Overall Structure and Active Site of HheG. To investigate possible structural determinants of the unique substrate scope of HheG, we determined the crystal structure of HheG at 2.3 Å resolution (see the Supporting Information). As found previously for other HHDHs, HheG forms a stable homotetramer (Figure 4A). The monomer exhibits a Rossmann-fold-like architecture characterized by a central seven-stranded parallel β-sheet (β_1–β_7) flanked by eight α-helices (Figure 4B). The active site of HheG is located in a long and deep cleft (Figure 5A) formed between the helices α_4 and α_5 and the helix–turn–helix motif involving helices α_6 and α_7. The catalytic triad comprised of Ser152, Tyr165, and Arg169 can be found at the bottom of this partially electropositive cleft (Figure 6). Ser152 is located in a flexible loop region between the 3_{10}-helix η_1 and the fifth β-strand, while Tyr165 and Arg169 are at the *C*-terminal pole of α_5. In the structure of HheG, the strongly electropositive halide binding site is occupied by a water molecule, which is coordinated by the side chain of Thr195 (Figure 4C).

Residual electron density was observed in proximity of the catalytic residue Ser152 (Figure S2 in the Supporting Information). This unattributed density, which superposes with the binding site of ligands from other HHDH structures, was also observed in the presence of reducing agent and in several structures obtained from different crystallization conditions of varying pH from 4.5 to 8.5. The quality of the electron density maps does not allow unambiguous identification of the bound compounds, which have likely been

DOI: 10.1021/acscatal.7b01854
ACS Catal. 2017, 7, 6877–6886

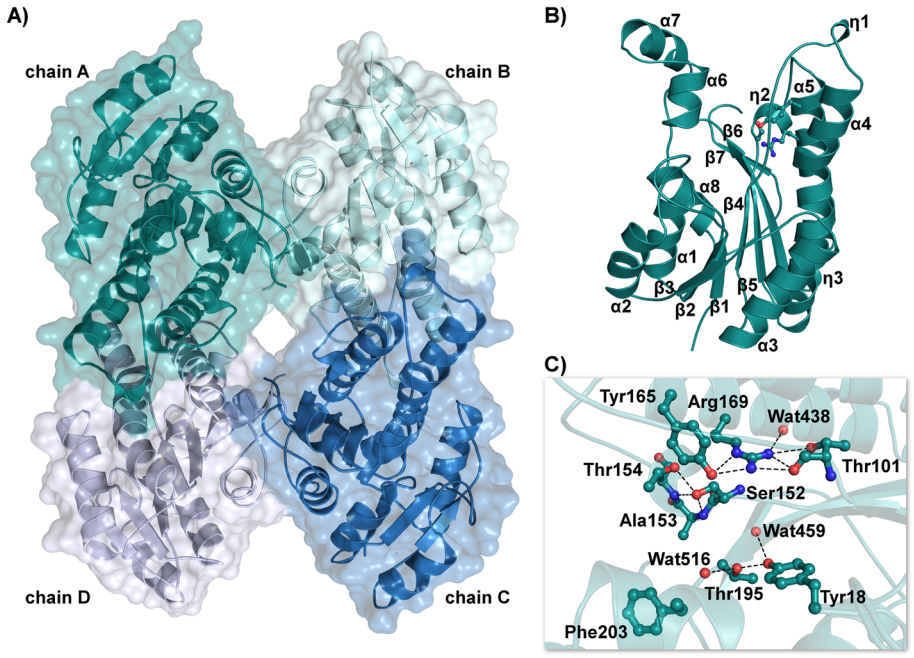

Figure 4. (A) Tetrameric biological assembly of the halohydrin dehalogenase HheG from *Ilumatobacter coccineus* shown as cartoon and surface representations. The individual chains are depicted in different colors. (B) Secondary structure elements within the Rossmann-fold-like architecture of a HheG monomer. The residues constituting the catalytic triad, Ser152, Tyr165, and Arg169, are highlighted as balls and sticks. (C) Close-up on the active site of HheG comprised of the catalytic triad shown with its hydrogen-bonding network (- - -), as well as the additional residues Thr195 and Phe203 with the former coordinating the water molecule (Wat516) occupying the halide binding site.

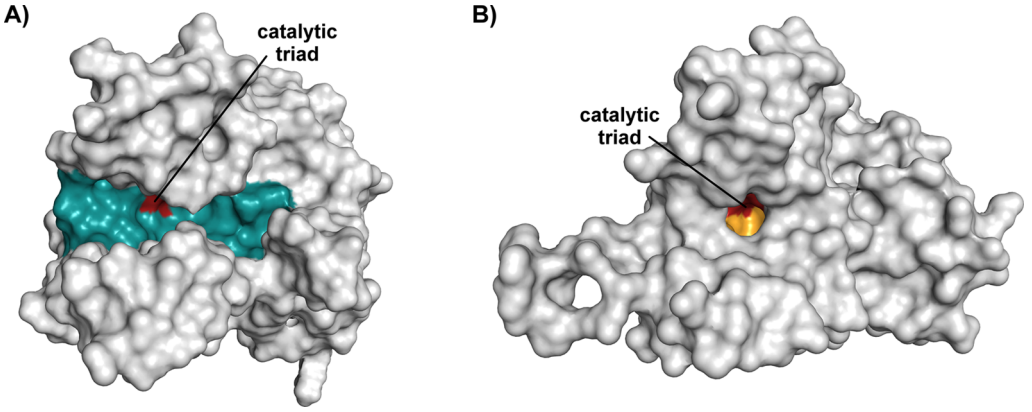

Figure 5. Surface representation of HheG from *I. coccineus* and HheC (mutant) from *A. tumefaciens* (PDB entry: 3ZN2),[25] respectively. (A) In HheG the active site harboring the catalytic triad (highlighted in red) is located in a large open cleft shown in teal. (B) In HheC, a narrow tunnel (shown in yellow) is leading to the active site with the catalytic triad highlighted in red.

copurified with the recombinant protein. Their presence, however, may explain why all attempts to cocrystallize HheG with substrates **1**, **2**, and **5** were unsuccessful.

Structural Comparison to Related HHDHs. A comparison of the structure of HheG with 14 previously published HHDH structures yields rmsd values on C_α positions ranging from 1.47 (PDB entry: 3ZN2) to 1.71 Å (PDB entry: 4Z9F). The overall folds of all HHDHs, including HheG, are rather similar and resemble the characteristic Rossmann fold that is found in all members of the SDR family. However, marked differences exist between HheG and the other members of this enzyme class. In general, HheG features a seventh β-strand which can be found in HheA and HheC as well but which is missing in HheB. Similar to the case for HheA and HheB, HheG lacks an extended C-terminus which can be found only in HheC (Figure S3A in the Supporting Information), where it reaches into the active site of an adjacent monomer via a conserved tryptophan residue.[27]

The most distinct differences between HheG and other HHDHs, however, are the shape and size of the active site pocket. While HheC, HheB, and HheA have rather narrow substrate tunnels leading to the active site,[28] HheG features a large open cleft (Figure 5). Using the program KVFinder[29] the volume of this active site cleft was calculated to be ~520 Å^3. As a comparison, the active site pocket in HheC (PDB entry: 3ZN2) is only 190 Å^3 (Figure S4 in the Supporting Information). The loop spanning residues His37 to Phe52, which is not present in the other structures and connects the β_2 strand to helix α_2, delimits the active site cleft of HheG on one side. Consequently, the α_2 helix, not present in HheB

DOI: 10.1021/acscatal.7b01854
ACS Catal. 2017, 7, 6877−6886

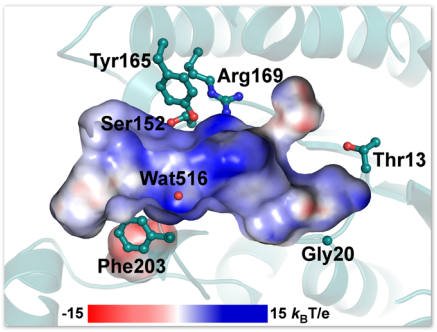

Figure 6. Close-up of the electropositive active site pocket of HheG. The electrostatic potential was calculated using the ABPS plugin[26] of PyMOL and is represented on the molecular surface with a scale ranging from −15 (red) to 15 (blue) k_bT/e. The residues of the catalytic triad Ser152, Tyr165, and Arg169 and the conserved residues Thr13 and Gly20, as well as Phe203 and the water molecule occupying the halide binding site (Wat516), are shown as balls and sticks.

structures, adopts an atypical position almost parallel to α_1 (Figure S3A in the Supporting Information). Another important structural feature that determines the shape of the active site pocket of HheG is helix α_6. This helix is longer in HheG, while in the other HHDH structures it corresponds to a loop that closes the active site. In the latter structures, an aromatic residue (Tyr185 in HheA2, Tyr169 in HheB from *Corynebacterium* sp. N-1074, or Phe186 in HheC) is mainly responsible for delimiting the active site tunnel within this region (loop) together with the residues of the catalytic triad and an additional conserved aromatic residue (Phe12 in HheC and HheA2 or Tyr19 in HheB). Not only is the corresponding residue Phe203 in the α_6 helix of HheG displaced by at least 2.0 Å (regarding C_α positions) in comparison to HheA2, HheB, or HheC but also its side chain is flipped away from the active site by ∼180°. As such, it occupies the position which in related halohydrin dehalogenases is occupied by an adjacent aromatic residue (Phe170 in HheB, Phe186 in HheA2, or Tyr187 in HheC), inducing an opening of the active site. Further, the conserved aromatic residue Tyr18 is displaced by at least 2.4 Å (regarding C_α positions) in comparison to the corresponding residues in structures of HheA2/HheC or HheB. This displacement leads to additional widening of the active site cleft of HheG (Figure S3B). While it cannot be excluded that substrate binding induces a movement of α_6 or at least a flip of Phe203 to close the active site, such a conformational change has not been observed in other HHDHs. It might be speculated that such substrate-induced conformational changes, on the other hand, could account for the observed cooperative behavior of HheG. Further biochemical and structural investigations, however, will be necessary to explain the observed cooperativity in the future.

Overall, we propose that the large active site cleft, in comparison to the narrow active site pockets in related HHDHs, explains why HheG preferentially converts cyclic epoxides over smaller aliphatic substrates. At the same time, this observation may indicate that the enzyme is able to accommodate even larger or sterically more demanding substrate molecules. The large epoxide *trans*-stilbene oxide, however, was not converted by HheG in previous tests.[12]

HheG Homologues. Using our motif-driven sequence database search, we recently identified a close homologue of HheG.[1] The enzyme from *Ilumatobacter nonamiensis* (HheG2) displays 74% sequence identity to HheG and was therefore also studied for its activity on cyclic epoxides **2** and **5**. Using 0.4 mg mL^{-1} purified enzyme in reactions with 20 mM substrate and 40 mM nucleophile (NaN_3 and NaCN), products **3**, **4**, and **6** were obtained in 39, 99, and 79% conversion, respectively, after overnight incubation at room temperature. HheG2 displayed also some enantioselectivity in the conversion of **2**, giving cyanoalcohol **3** with 22% ee and azidoalcohol **4** with 41% ee, which are comparable to the data obtained for HheG. Hence, the ability to convert cyclic epoxides is not exclusive to HheG but might likely represent a general feature of G-type HHDH subfamily members. To verify this hypothesis, a PHI-BLAST database search for potential HheG homologues in the most recent GenBank release 220 was performed using our previously published HHDH sequence motifs[11] with HheG as the query sequence. However, no additional member of the G-type subfamily could be identified. Thus, it remains to be examined whether further HheG homologues will exhibit the same substrate preference for cyclic epoxides.

CONCLUSION

HheG from *Ilumatobacter coccineus* is special among other halohydrin dehalogenases, as it can be applied in the conversion of sterically demanding cyclic epoxides while its activity toward standard HHDH substrates is comparably low. Using this enzyme, different cyclic β-substituted alcohols such as 2-azido- and 2-cyano-1-cyclohexanols can be accessed, which are even formed with moderate enantiomeric excess. With this, HheG broadens the versatility of the HHDH enzyme toolbox for biocatalytic routes toward fine chemicals and pharmaceutical synthons. For future practical applications, however, enzyme optimization is still required. Especially the enzyme's activity with cyanide, its enantioselectivity, and its stability have to be enhanced by protein engineering, which is subject to current investigation in our group. The crystal structure of HheG reported here aids in explaining the substrate preference of this enzyme, as its active site is positioned in a wide-open cleft, which is in contrast to rather buried active sites found in other HHDH structures. Additionally, this structure will substantially facilitate further protein engineering campaigns of HheG and its close homologue HheG2, which also exhibits activity toward cyclic epoxides.

EXPERIMENTAL SECTION

Chemicals. All chemicals were of analytical or the highest available grade. Substrates 2-chlorocyclohexanol (**1**), (+)-*cis*-/(+)-*trans*-limonene oxide (**5**) and (+)-*trans*-limonene oxide ((+)-*trans*-**5**) were purchased from Sigma-Aldrich; cyclohexene oxide (**2**) and *trans*-2-hydroxycyclohexane-1-carbonitrile (**3**) were obtained from Acros Organics.

Bacterial Strains, Plasmids, and Enzymes. *E. coli* BL21(DE3) Gold (Life Technologies, Darmstadt, Germany), *E. coli* C43(DE3) (Lucigen Corporation, Middleton, WI, USA), and *E. coli* Top10 (Life Technologies) were used as hosts for heterologous protein production. pET-28a-based vectors harboring a T7 promoter and resulting in N-terminal hexahistidine (His_6) tag fusion were used for expression of HHDH genes.[11] Vector pBAD-*hheC* harboring an *ara* promotor was used for the expression of the HheC gene.[30]

Enzyme Expression and Purification. Heterologous enzyme production of HHDHs was carried out as reported previously.[12] For the production of recombinant HheG, 500

DOI: 10.1021/acscatal.7b01854
ACS Catal. 2017, 7, 6877−6886

mL TB medium (4 mL L^{-1} glycerol, 12 g L^{-1} peptone, 24 g L^{-1} yeast extract, 0.17 M KH_2PO_4, 0.74 M K_2HPO_4) supplemented with 50 mg L^{-1} kanamycin and 0.2 mM IPTG was inoculated with 10% (v/v) overnight culture of *E. coli* BL21(DE3) pET-28a-*hheG* and incubated for 24 h at 22 °C. Cells were harvested by centrifugation (4400*g*, 20 min at 4 °C), and the cell pellet was stored at −20 °C until further use.

Purification of HheG was carried out by affinity chromatography. A frozen cell pellet was resuspended in buffer A (50 mM Tris·SO_4, 500 mM Na_2SO_4, 25 mM imidazole, pH 7.9), containing 1 mg mL^{-1} lysozyme and 100 μM phenylmethylsulfonyl fluoride as protease inhibitor. Cells were disrupted by sonication (six cycles of 1 min at an amplitude of 60% and 1 min pause, on ice), and the resulting crude extract was centrifuged (16600*g*, 30 min, 4 °C) to obtain HheG-containing cell free extract (CFE). This CFE was filtered through a 0.45 μm cellulose acetate membrane filter (Sarstedt, Nümbrecht, Germany) and loaded (flow rate 2 mL min^{-1}) on a 5 mL HisTrap FF column (GE Healthcare, Freiburg, Germany) pre-equilibrated with buffer A using an Äkta FPLC system (GE Healthcare). To remove nonspecifically bound proteins, the column was washed with five column volumes of buffer A at a flow rate of 5 mL min^{-1}. Elution of target protein was achieved using a 100 mL gradient of 25−500 mM imidazole in buffer A (flow rate 2 mL min^{-1}). Fractions containing target protein HheG were identified by SDS-PAGE. Fractions of highest purity were pooled and concentrated by ultrafiltration using Amicon Ultra-15 centrifugal filter units with 10 kDa NMWL (Merck Millipore, Darmstadt, Germany). Afterward, the concentrated purified protein was desalted using a PD-10 column (GE Healthcare) and TE buffer (10 mM Tris·SO_4, pH 7.9, 4 mM EDTA). Protein concentration was measured on a NanoDrop 1000 spectrophotometer (Thermo Scientific, Waltham, MA, USA) at 280 nm using a molar extinction coefficient for His-tagged HheG of 15470 M^{-1} cm^{-1} and a molecular weight of 29881 Da.

For crystallization studies, HheG was expressed and purified as described above using an additional size-exclusion chromatography step. After affinity chromatography, the collected fractions were loaded on a HiLoad 26/600 Superdex 200 pg column (GE Healthcare) and HheG was eluted with crystallization buffer (see below), applying a flow of 2 mL min^{-1}.

Selenomethionine-labeled HheG (SeMet His_6-HheG) was produced as described above but using minimal media (M9) containing 60 mg L^{-1} selenomethionine. Protein purification was carried out using a protocol similar to that described above.

Bioconversion of Cyclic Epoxides using 17 HHDHs. Conversion of cyclic epoxides **2** and **5** by 17 different HHDHs was tested on a small scale and analyzed by gas chromatography (GC) and GC coupled with mass spectrometry (GC-MS). Reactions were performed in a total volume of 1 mL in 50 mM Tris·SO_4 buffer, pH 8.0, at room temperature with 20 mM sodium azide (NaN_3) using 150 μg of each HHDH and 5 mM of substrate **2** or **5**. Respective negative control reactions without enzyme but with only substrate with NaN_3 were carried out in parallel. After 24 h, 0.5 mL samples of each reaction mixture were withdrawn and extracted using an equivalent volume of *tert*-butyl methyl ether (TBME) supplemented with 0.1% (v/v) dodecane as internal standard. After the organic extracts were dried over anhydrous $MgSO_4$, samples were injected on GC for quantification and on GC-MS for product identification.

Temperature and pH Profiles of HheG. To determine HheG's temperature and pH optima, reactions were carried out in 0.5 mL using 20 mM **2**, 40 mM NaN_3, and 0.4 mg mL^{-1} HheG. Temperature profile reactions were performed in 50 mM Tris·SO_4, pH 8.0, buffer at temperatures ranging from 4 to 90 °C. After 30 min, 500 μL of TBME containing 0.1% (v/v) dodecane was added to each of the reaction mixtures for extraction. In case of pH profiles, buffers of varying pH were used (50 mM citrate buffer at pH 4.0−6.5, 50 mM sodium phosphate buffer at pH 6.0−8.0, 50 mM Tris·SO_4 buffer at pH 7−9, and glycine NaOH buffer at pH 8−11) and reaction mixtures were extracted after incubation at 30 °C for 40 min using 500 μL of TBME containing 0.1% (v/v) dodecane. Product formation was followed by gas chromatography. Negative control reactions without enzyme were performed in parallel to determine the chemical background of epoxide ring-opening. Negative controls and reactions containing enzyme were carried out in duplicate, and the chemical background was subtracted from enzymatic conversions. In temperature and pH profile tests, the highest observed conversion in the sample series was set to 100%.

Steady-State Kinetics of HheG. Enzyme kinetics of HheG toward chloroalcohol **1** were determined by monitoring halide release[12] in microtiter-plate format using a CLARIOstar spectrophotometer (BMG Labtech, Ortenberg, Germany). Dehalogenation reactions were performed in 25 mM Tris·SO_4 buffer at pH 7 containing 0.5−150 mM substrate **1** in a total volume of 1.5 mL. The reaction mixtures were incubated at 30 °C after 100 μg mL^{-1} HheG was added. To calculate initial activities, 100 μL of each sample was withdrawn after 0.5, 1.5, 2.5, 3, 4, 5, 6, 10, 15, 20, 30, and 60 min and mixed with 100 μL of assay reagent (equal volumes of solution I (0.25 M $NH_4Fe(SO_4)_2$ in 9 M HNO_3) and solution II (saturated solution of $Hg(SCN)_2$ in absolute ethanol)). Absorbance at 460 nm was measured immediately, and the resulting dehalogenase activities were calculated using a standard curve for Cl^- in the range of 0−2 mM. Activities were calculated in μmol min^{-1}, plotted against the substrate concentration, and fitted according to the Hill equation for cooperative binding (eq 1)

$$V = \frac{V_{max}[S]^{n_H}}{(K_{50})^{n_H} + [S]^{n_H}} \quad (1)$$

where V is the reaction velocity, V_{max} the maximum velocity of the reaction, $[S]$ the substrate concentration, K_{50} the substrate concentration at half-maximal reaction velocity, and n_H the Hill coefficient. Chemical background activities in control reactions containing no enzyme were subtracted before fitting.

In the case of epoxide ring-opening of substrates **2** and **5**, reactions were analyzed by GC. Kinetic constants of HheG for ring-opening of **2** were determined using either NaCN or NaN_3 as nucleophile at fixed concentrations of 75 and 50 mM, respectively. Kinetic constants of HheG for ring opening of **5** were determined using 50 mM NaN_3 as nucleophile. Reactions were carried out in 1.6 mL of 50 mM Tris·SO_4 buffer at a pH of 8 containing 5−150 mM **2** and 300 μg mL^{-1} (in the case of NaCN) or 156.25 μg mL^{-1} (in the case of NaN_3) HheG at 22 °C. After 10, 30, 60, and 90 min, each 400 μL sample was taken and extracted with 400 μL of TBME containing 0.1% (v/v) dodecane. Product formation was quantified by GC on the basis of a standard curve for product **3** or via substrate depletion in the case of azidoalcohol **4**. Activities were

DOI: 10.1021/acscatal.7b01854
ACS Catal. 2017, 7, 6877−6886

calculated in μmol min^{-1}, plotted, and fitted as described above. Chemical background activities in control reactions without enzyme were subtracted before fitting.

K_{50} values for the nucleophiles cyanide (NaCN) and azide (NaN_3) were determined in reactions with a total volume of 1.6 mL in 50 mM Tris·SO_4 buffer at a pH of 8 containing 5−150 mM nucleophile, 10 mM **2**, and 300 or 156.25 μg mL^{-1} HheG, respectively. After 30 min, 90 min, 4 h, and 24 h (NaCN) or 10, 30, 60, and 90 min (NaN_3), each 400 μL sample was taken, extracted as described above, and analyzed by GC. Activities (in μmol min^{-1}) were calculated, plotted, and fitted as described above. Chemical background activities in control reactions without enzyme were subtracted before fitting.

For preparation of a NaCN stock solution, NaCN salt was dissolved in 10 mM NaOH solution and stored in a closed vial. High pH of the stock solution is required to prevent formation of toxic HCN gas. Additionally, all reactions using CN^- as nucleophile were handled in a ventilated fume hood with HCN gas monitoring present.

Stereoselectivity Determination. Conversion of cyclohexene oxide (**2**) to the chiral products *trans*-2-hydroxycyclohexane-1-carbonitrile (**3**) and 2-azidocyclohexan-1-ol (**4**) was followed using achiral and chiral GC. Reactions were performed using 0.25 mg mL^{-1} HheG, 20 mM NaCN or NaN_3, respectively, and 5 mM substrate **2** in a total volume of 2 mL of 50 mM Tris·SO_4, pH 8. Each 0.5 mL sample was taken after 0.5, 2, and 24 h and extracted using 500 μL of TBME containing 0.1% (v/v) dodecane. Conversion (percent) was calculated on the basis of peak areas from achiral GC analysis, and product enantiomeric excess (ee_P in percent) was determined by chiral GC analysis.

To distinguish the enantiomers of **3** on chiral GC, an enzymatic kinetic resolution of **3** was carried out using lipase PS from *Pseudomonas cepacia* (Sigma-Aldrich) and vinyl acetate as an acyl donor as described elsewhere.[22,23] A reaction in 3 mL volume was performed using 100 mg of lipase PS, 100 mM commercial *trans*-2-hydroxycyclohexane-1-carbonitrile (**3**), 200 mM vinyl acetate in TBME at 22 °C, and shaking at 800 rpm. Samples were taken after 1.5 h and after overnight incubation and injected on chiral GC.

For determination of the preferentially formed enantiomer of **4**, the product obtained in a HheG-catalyzed azidolysis of **2** was reduced chemically to 2-aminocyclohexan-1-ol, for which enantiopure 1*R*,2*R* and 1*S*,2*S* product standards are available (Sigma-Aldrich). Production of **4** was carried out using 30 mL of HheG overexpressing *E. coli* cells with an OD_{600} value of 40 using 50 mM **2** and 100 mM NaN_3 in 50 mM Tris·SO_4 buffer, pH 8. The reaction mixture was incubated at 22 °C for 24 h and stirred at 800 rpm. Afterward, the reaction mixture was extracted three times using 30 mL of ethyl acetate. The combined organic extracts were dried over Na_2SO_4, and solvent was removed by evaporation. Approximately 0.75 mmol of **4** were dissolved in a 1/1 solution of methanol and ethyl acetate for subsequent chemical reduction of azidoalcohol **4**. For in situ production of hydrogen, 1.7 mL of triethylsilane was added to the mixture. As catalyst, 0.03 g of palladium on carbon was added and the reduction reaction was carried out for 90 min at room temperature. Afterward, the catalyst was removed by centrifugation and the solvent was evaporated under reduced pressure. The resulting aminoalcohol was dissolved in pyridine, derivatized using trifluoroacetic anhydride (incubation for 1 h at 65 °C), and analyzed by chiral GC.

Whole-Cell Biotransformations and Cascade Reactions. For whole-cell conversions, HheG was heterologously expressed in *E. coli* BL21(DE3) pET-28a-*hheG* as mentioned above. Cells containing empty pET-28a vector were used as a negative control. For cyanolysis of epoxide **2**, frozen cells were resuspended in 50 mM Tris·SO_4 buffer, pH 8, containing 20 mM **2** and 40 mM NaCN to reach a final OD_{600} value of 40. For cascade reactions from chloroalcohol **1** to cyanoalcohol **3** via dehalogenation of **1** and cyanolysis of intermediate **2**, frozen cells were resuspended in 50 mM Tris·SO_4 buffer, pH 8, containing 20 mM **1** and 40 mM NaCN to reach a final OD_{600} value of 40. All reaction mixtures were incubated at room temperature with constant stirring (800 rpm). A 500 μL sample was taken after 1, 3, 24, 48, and 120 h, extracted, and analyzed using achiral and chiral GC. Product yields were calculated using a standard curve for cyanoalcohol **3**.

For the conversion of (+)-*cis*-/(+)-*trans*-**5** using whole cells, reactions were carried out as described but using 20 mM **5** and 40 mM NaN_3 as substrate and nucleophile, respectively. Samples were taken after 1, 2, and 24 h incubation at room temperature with stirring (800 rpm) and analyzed on achiral GC after extraction. Conversion (percent) was calculated on the basis of relative peak areas.

To determine the regioselectivity of HheG in the conversion of (+)-*trans*-**5**, a whole-cell biotransformation was performed on a preparative scale and the resulting product **6** was purified to homogeneity. In total, 40 mM (+)-*trans*-**5** (600 mg) was converted using 80 mM NaN_3 in 10 mL of 50 mM Tris·SO_4 buffer, pH 8, containing HheG-overexpressing *E. coli* cells at OD_{600} = 40. The reaction mixture was incubated for 24 h at 22 °C. A 500 μL sample was extracted using TBME (0.1% (v/v) dodecane) and analyzed by GC to determine conversion. For purification of product **6**, the whole reaction mixture was extracted three times with each 10 mL of dichloromethane (DCM) and the resulting crude product was purified by silica gel chromatography with a gradient from 50% to 100% DCM in pentane. The purified product was obtained as a colorless oil in 34% yield (212.1 mg).

*(+)-trans-2-Azido-1-methyl-4-(prop-1-en-2-yl)cyclohexan-1-ol ((+)-trans-**6a**).* $[\alpha]^{21}_D$ = +124.8. ^{1}H NMR (600 MHz, DMSO-d_6): δ 4.70−4.68 (m, CH_2; 2H), 4.65−4.64 (s, OH; 1H), 3.56−3.55 (m, CH, 1H), 2.05−1.99 (tt, ^3J = 11.9, 3.2 Hz, CH, 1H), 1.94−1.88 (ddd, J = 13.6, 12.0, 3.0 Hz, CH_2 1 H), 1.68 (s, CH_3, 3 H), 1.68−1.63 (m, CH_2, 1H), 1.57−1.49 (ddd, J = 23.6, 12.0, 4.5 Hz, CH_2, 1H) 1.47−1.41 (m, CH_2, 2H) 1.41−1.35 (m, CH_2, 1H), 1.12 (s, CH_3, 3H). ^{13}C NMR (151 MHz, DMSO-d_6): δ 149.0 (C_q), 109.1 (CH_2), 69.0 (C_q), 66.2 (CH), 37.9 (CH), 33.6 (CH_2), 30.2 (CH_2), 27.4 (CH_3), 25.6 (CH_2), 20.8 (CH_3). ESI-HRMS: [M + Na^+] m/z 218.12648 (calculated [M + Na^+] m/z 218.12638).

Analytical Methods. Achiral and chiral GC analyses were performed on a GC2010 plus gas chromatograph (Shimadzu, Duisburg, Germany) with FID detection. Achiral separation was carried out using a OPTIMA 5 MS column (Macherey Nagel, Düren, Germany) with a length of 30 m, an inner diameter of 0.25 mm, and a film thickness of 0.25 μm. Separation of substrates and products was achieved using two different temperature programs: program 1 (100 °C, 3 min//50 °C min^{-1}//200 °C//20 °C min^{-1}//300 °C, 2.5 min) for compounds **1**−**4** and program 2 (80 °C, 1 min//10 °C min^{-1}//160 °C//20 °C min^{-1}//300 °C) for compounds **5** and **6** with a total flow of 1 mL min^{-1} and hydrogen as carrier gas. The substrates eluted at retention times of 4.6 min (**1**), 3.3 min

DOI: 10.1021/acscatal.7b01854
ACS Catal. 2017, 7, 6877−6886

(**2**), 7.3 min (*cis*-**5**), and 7.4 min (*trans*-**5**), while the products eluted at 5.6 min (**3**), 5.5 min (**4**), 10.9 min (*cis*-**6**), and 11.3 min (*trans*-**6**). Chiral separation was carried out using two different chiral columns, LIPODEX E and HYDRODEX γ-DIMOM (Macherey-Nagel), each with a length of 25 m, an inner diameter of 0.25 mm, and a film thickness of 0.25 μm. Enantiomers were separated on the Lipodex E column using a temperature program of 80 °C, 5 min//10 °C min^{-1}//110 °C, 5 min//2 °C min^{-1}//180 °C, 5 min with a total flow of 0.8 mL min^{-1} and hydrogen as carrier gas. Retention times were as follows: *rac*-**1** (9.5 and 9.7 min), **2** (2.6 min), (1*R*,2*S*)-2-cyanocyclohexyl acetate (21.6 min), (1*S*,2*S*)-**4** (17.8 min), (1*R*,2*R*)-**4** (18.1 min), (1*R*,2*S*)-**3** (30.6 min), and (1*S*,2*R*)-**3** (31.0 min). Enantiomers on the Hydrodex γ-DIMOM column were separated using a temperature program of 60 °C, 30 min//10 °C min^{-1}//195 °C, 5 min with a total flow of 3.27 mL min^{-1} and hydrogen as carrier gas. Retention times were as follows: (1*R*,2*R*)-2-aminocyclohexan-1-ol (26.6 min) and (1*S*,2*S*)-2-aminocyclohexan-1-ol (27.4 min).

GC-MS analysis of (+)-*trans*-**6a** was performed on a GCMS-QP2010SE (Shimadzu) instrument equipped with a ZB-5MS GUARDIAN column (30 m × 0.25 mm, 0.25 μm film thickness). The product (+)-*trans*-**6a** was dissolved in diethyl ether. The injector temperature was set to 250 °C and interface temperature to 280 °C. Helium was used as carrier gas with a flow of 1.5 mL min^{-1}, and separation was performed with 50 °C, 3 min//12 °C min^{-1}//300 °C, 8 min as the temperature program. The product was detected at a retention time of 12.6 min with *m*/*z* 195 (calculated $[M]^+$ *m*/*z* 195).

Mass spectrometric analysis of (+)-*trans*-**6a** was carried out in diethyl ether using ESI-HRMS on a LTQ-Orbitrap Velos spectrometer (ThermoFisher Scientific, Bremen, Germany).

Localization of the carbon−nitrogen bond (C−N_3) in (+)-*trans*-**6a** was determined by NMR (AV ll-600, Bruker, Billerica, MA, USA) for which different 2D correlation spectra (^{1}H−^{1}H COSY, ^{1}H−^{1}H HMBC, NOESY, and ^{1}H−^{15}N HMBC) were determined using deuterated dimethyl sulfoxide as solvent.

A solution of (+)-*trans*-**6a** in DCM (*c* = 10 mg mL^{-1}) was analyzed with a polarimeter (Propol Digital Automatic Polarimeter, Dr. Kernchen, Seelze, Germany) to obtain the specific rotation value.

Crystallization and Data Collection. Crystallization experiments of N-terminally hexahistidine-tagged HheG wild type at 14 mg mL^{-1} and selenomethionine derivatized (SeMet) His_6-HheG at 24 mg mL^{-1}, both in 10 mM Tris·SO_4 buffer, pH 8.0, containing 2 mM EDTA and 5 mM β-mercaptoethanol were carried out via the sitting-drop vapor diffusion method at room temperature in 96-well INTELLI-PLATES (ARI - Art Robbins Instruments, Sunnyvale, CA, USA) using a nano-dispensing robot (Honeybee 963, Genomic Solutions, Huntingdon, U.K.) and commercial sparse matrix screening suites. Drops consisting of 200 nL of protein solution and 200 nL of precipitant were equilibrated against a 60 μL reservoir.

Crystals of native HheG were obtained within a few days from a condition of the WIZARDS I+II screening suite (Emerald Biosystems Inc., Bainbridge Island, WA, USA), comprised of 0.1 M sodium acetate pH 4.5 and 1 M ammonium phosphate dibasic. SeMet His_6-HheG crystallized under conditions comprising 0.1 M imidazole pH 8.0, 0.2 M lithium sulfate, and 10% (w/v) PEG 3000.

For both native and derivatized protein, hexagonal prism shaped crystals of approximately 90 μm length and 150 μm diameter were cryoprotected by addition of 25% (v/v) glycerol to their respective mother liquors, mounted on nylon loops, and flash-frozen in liquid nitrogen. Diffraction data were collected at 100 K at beamline X06DA (PXIII) at the Swiss Light Source of the Paul Scherrer Institute on a PILATUS 2M-F hybrid-pixel detector (DECTRIS Ltd., Baden-Daettwil, Switzerland).

Indexing and integration of all diffraction data was performed using XDS.[31] For scaling the programs AIMLESS[32] of the CCP4 suite[33] and Xscale were used for the native and anomalous data sets, respectively. Statistics of the data sets are presented in Table S1 in the Supporting Information.

Structure Determination and Refinement. Initial phases for HheG could be obtained using SAD and the anomalous signal of selenium extending to 2.7 Å. Overall, 108 selenium sites were located using SHELXD[34] and, after density modification and phase extension to 2.3 Å using the native data set and SHELXE,[34] the initial phases were provided to phenix.autobuild,[35] which built approximately 65% (1838 residues) of the 10 HheG copies constituting the asymmetric unit of the crystal. Further model building and refinement were carried out by alternating rounds of manual adjustment in COOT[36] and maximum likelihood refinement in phenix.refine[37] of the PHENIX software suite.[38] Structural flexibility was modeled using Translation/Libration/Screw refinement.[39] In the last step of refinement, water molecules were attributed to their nearest TLS group using a script developed by Reichelt and Blankenfeldt (unpublished). Refinement statistics of the final model are reported in Table S1 in the Supporting Information. Final structure validation was done with MolProbity.[40] Diffraction data and coordinates have been deposited in the Protein Data Bank (PDB entry: 5O30).[41] All structural illustrations were generated using the PyMOL Molecular Graphics System version 1.8.4 (Schrödinger, LLC, New York City, NY, USA).

Database Search for HheG Homologues. A PHI-BLAST[42] search in the nr and env_nr databases of GenBank (release 220) was performed using the combination of two previously reported HHDH sequence motifs: T-X_4-(F/Y)-X-G-X_{50-150}-S-X_{12}-Y-X_3-R and the HheG protein sequence (GenBank accession number AMQ13576.1) as query. A distance tree of the obtained hits was generated on the basis of the neighbor joining method and inspected for new members of the HHDH G-type subfamily.

■ ASSOCIATED CONTENT

Supporting Information

The Supporting Information is available free of charge on the ACS Publications website at DOI: 10.1021/acscatal.7b01854.

pH and temperature profiles and additional structural information (PDF)

■ AUTHOR INFORMATION

Corresponding Author

*A.S.: tel, +49 531 391-55400; fax, +49 531 391-55401; e-mail, a.schallmey@tu-braunschweig.de.

ORCID

Anett Schallmey: 0000-0002-6670-0574

Present Addresses

[§]Institute of Chemistry and Biotechnology, Competence Center for Biocatalysis, Zurich University of Applied Sciences, Einsiedlerstrasse 31, 8820 Wädenswil, Switzerland.

DOI: 10.1021/acscatal.7b01854
ACS Catal. 2017, 7, 6877−6886

[‖]Department of Molecular Biology, Max-Planck-Institute for Biophysical Chemistry, Max Planck Society, Am Fassberg 11, Göttingen 37077, Germany.

Notes

The authors declare no competing financial interest.

■ ACKNOWLEDGMENTS

We thank Dr. Marcus Schallmey for technical assistance with chiral GC analysis and suggestions on the manuscript. Furthermore, we thank Dr. Rainer Wardenga from Enzymicals AG (Greifswald, Germany) for scientific collaboration and discussion of the biocatalytic data. The authors also thank the staff at beamline PXIII (X06DA) of the Swiss Light Source (PSI, Villingen, Switzerland), in particular Dr. Meitian Wang, for beamline access and support. This work was financially supported by the German Federal Ministry for Economic Affairs and Energy (BMWi) within the AIF-ZIM funding scheme (award numbers KF3041401 and KF2584302).

■ REFERENCES

(1) Schallmey, A.; Schallmey, M. *Appl. Microbiol. Biotechnol.* **2016**, *100*, 7827−7839.
(2) Castro, C. E.; Bartnicki, E. W. *Biochemistry* **1968**, *7*, 3213−3218.
(3) Ma, S. K.; Gruber, J.; Davis, C.; Newman, L.; Gray, D.; Wang, A.; Grate, J.; Huisman, G. W.; Sheldon, R. A. *Green Chem.* **2010**, *12*, 81−86.
(4) Fox, R. J.; Davis, S. C.; Mundorff, E. C.; Newman, L. M.; Gavrilovic, V.; Ma, S. K.; Chung, L. M.; Ching, C.; Tam, S.; Muley, S.; Grate, J.; Gruber, J.; Whitman, J. C.; Sheldon, R. A.; Huisman, G. W. *Nat. Biotechnol.* **2007**, *25*, 338−344.
(5) Lutje Spelberg, J. H.; Tang, L.; Kellogg, R. M.; Janssen, D. B. *Tetrahedron: Asymmetry* **2004**, *15*, 1095−1102.
(6) Elenkov, M. M.; Tang, L.; Meetsma, A.; Hauer, B.; Janssen, D. B. *Org. Lett.* **2008**, *10*, 2417−2420.
(7) Mikleušević, A.; Hameršak, Z.; Salopek-Sondi, B.; Tang, L.; Janssen, D. B.; Majerić Elenkov, M. *Adv. Synth. Catal.* **2015**, *357*, 1709−1714.
(8) Elenkov, M. M.; Hoeffken, H. W.; Tang, L.; Hauer, B.; Janssen, D. B. *Adv. Synth. Catal.* **2007**, *349*, 2279−2285.
(9) Fuchs, M.; Simeo, Y.; Ueberbacher, B. T.; Mautner, B.; Netscher, T.; Faber, K. *Eur. J. Org. Chem.* **2009**, *2009*, 833−840.
(10) van Hylckama Vlieg, J. E. T.; Tang, L.; Spelberg, J. H. L.; Smilda, T.; Poelarends, G. J.; Bosma, T.; van Merode, A. E. J.; Fraaije, M. W.; Janssen, D. B. *J. Bacteriol.* **2001**, *183*, 5058−5066.
(11) Schallmey, M.; Koopmeiners, J.; Wells, E.; Wardenga, R.; Schallmey, A. *Appl. Environ. Microbiol.* **2014**, *80*, 7303−7315.
(12) Koopmeiners, J.; Halmschlag, B.; Schallmey, M.; Schallmey, A. *Appl. Microbiol. Biotechnol.* **2016**, *100*, 7517−7527.
(13) Elenkov, M. M.; Hauer, B.; Janssen, D. B. *Adv. Synth. Catal.* **2006**, *348*, 579−585.
(14) Hu, L. Y.; Du, D.; Hoffman, J.; Smith, Y.; Fedij, V.; Kostlan, C.; Johnson, T. R.; Huang, Y.; Kesten, S.; Harter, W.; Yue, W. S.; Li, J. J.; Barvian, N.; Mitchell, L.; Lei, H. J.; Lefker, B.; Carroll, M.; Dettling, D.; Krieger-Burke, T.; Samas, B.; Yalamanchili, R.; Lapham, K.; Pocalyko, D.; Sliskovic, D.; Ciotti, S.; Stoller, B.; Hena, M. A.; Ding, Q.; Maiti, S. N.; Stier, M.; Welgus, H. *Bioorg. Med. Chem. Lett.* **2007**, *17*, 5983−5988.
(15) Hasnaoui-Dijoux, G.; Majerić Elenkov, M.; Lutje Spelberg, J. H.; Hauer, B.; Janssen, D. B. *ChemBioChem* **2008**, *9*, 1048−1051.
(16) Tang, L.; Lutje Spelberg, J. H.; Fraaije, M. W.; Janssen, D. B. *Biochemistry* **2003**, *42*, 5378−5386.
(17) You, Z.-Y.; Liu, Z.-Q.; Zheng, Y.-G. *Appl. Microbiol. Biotechnol.* **2013**, *97*, 9−21.
(18) Yu, F.; Nakamura, T.; Mizunashi, W.; Watanabe, I. *Biosci., Biotechnol., Biochem.* **1994**, *58*, 1451−1457.
(19) Nakamura, T.; Nagasawa, T.; Yu, F.; Watanabe, I.; Yamada, H. *Appl. Environ. Microbiol.* **1994**, *60*, 1297−1301.
(20) Nagasawa, T.; Nakamura, T.; Yu, F.; Watanabe, I.; Yamada, H. *Appl. Microbiol. Biotechnol.* **1992**, *36*, 478−482.
(21) Vaidyanathan, R.; Hesmondhalgh, L.; Hu, S. *Org. Process Res. Dev.* **2007**, *11*, 903−906.
(22) Forró, E.; Lundell, K.; Fülöp, F.; Kanerva, L. T. *Tetrahedron: Asymmetry* **1997**, *8*, 3095−3099.
(23) Utczás, M.; Székely, E.; Forró, E.; Szőllősy, Á.; Fülöp, F.; Simándi, B. *Tetrahedron Lett.* **2011**, *52*, 3916−3918.
(24) Yao, P.; Wang, L.; Yuan, J.; Cheng, L.; Jia, R.; Xie, M.; Feng, J.; Wang, M.; Wu, Q.; Zhu, D. *ChemCatChem* **2015**, *7*, 1438−1444.
(25) Schallmey, M.; Jekel, P.; Tang, L.; Majerić Elenkov, M.; Höffken, H. W.; Hauer, B.; Janssen, D. B. *Enzyme Microb. Technol.* **2015**, *70*, 50−57.
(26) Baker, N. A.; Sept, D.; Joseph, S.; Holst, M. J.; McCammon, J. A. *Proc. Natl. Acad. Sci. U. S. A.* **2001**, *98*, 10037−10041.
(27) de Jong, R. M.; Tiesinga, J. J. W.; Rozeboom, H. J.; Kalk, K. H.; Tang, L.; Janssen, D. B.; Dijkstra, B. W. *EMBO J.* **2003**, *22*, 4933−4944.
(28) Watanabe, F.; Yu, F.; Ohtaki, A.; Yamanaka, Y.; Noguchi, K.; Yohda, M.; Odaka, M. *Proteins: Struct., Funct., Genet.* **2015**, *83*, 2230−2239.
(29) Oliveira, S. H. P.; Ferraz, F. A. N.; Honorato, R. V.; Xavier-Neto, J.; Sobreira, T. J. P.; de Oliveira, P. S. L. *BMC Bioinf.* **2014**, *15*, 197−204.
(30) Haak, R. M.; Tarabiono, C.; Janssen, D. B.; Minnaard, A. J.; de Vries, J. G.; Feringa, B. L. *Org. Biomol. Chem.* **2007**, *5*, 318−323.
(31) Kabsch, W. *Acta Crystallogr., Sect. D: Biol. Crystallogr.* **2010**, *66*, 133−144.
(32) Evans, P. R.; Murshudov, G. N. *Acta Crystallogr., Sect. D: Biol. Crystallogr.* **2013**, *69*, 1204−1214.
(33) Winn, M. D.; Ballard, C. C.; Cowtan, K. D.; Dodson, E. J.; Emsley, P.; Evans, P. R.; Keegan, R. M.; Krissinel, E. B.; Leslie, A. G. W.; McCoy, A.; McNicholas, S. J.; Murshudov, G. N.; Pannu, N. S.; Potterton, E. A.; Powell, H. R.; Read, R. J.; Vagin, A.; Wilson, K. S. *Acta Crystallogr., Sect. D: Biol. Crystallogr.* **2011**, *67*, 235−242.
(34) Sheldrick, G. M. *Acta Crystallogr., Sect. D: Biol. Crystallogr.* **2010**, *66*, 479−485.
(35) Terwilliger, T. C.; Grosse-Kunstleve, R. W.; Afonine, P. V.; Moriarty, N. W.; Zwart, P. H.; Hung, L. W.; Read, R. J.; Adams, P. D. *Acta Crystallogr., Sect. D: Biol. Crystallogr.* **2008**, *64*, 61−69.
(36) Emsley, P.; Lohkamp, B.; Scott, W. G.; Cowtan, K. *Acta Crystallogr., Sect. D: Biol. Crystallogr.* **2010**, *66*, 486−501.
(37) Afonine, P. V.; Grosse-Kunstleve, R. W.; Echols, N.; Headd, J. J.; Moriarty, N. W.; Mustyakimov, M.; Terwilliger, T. C.; Urzhumtsev, A.; Zwart, P. H.; Adams, P. D. *Acta Crystallogr., Sect. D: Biol. Crystallogr.* **2012**, *68*, 352−367.
(38) Adams, P. D.; Afonine, P. V.; Bunkóczi, G.; Chen, V. B.; Davis, I. W.; Echols, N.; Headd, J. J.; Hung, L.-W.; Kapral, G. J.; Grosse-Kunstleve, R. W.; McCoy, A. J.; Moriarty, N. W.; Oeffner, R.; Read, R. J.; Richardson, D. C.; Richardson, J. S.; Terwilliger, T. C.; Zwart, P. H. *Acta Crystallogr., Sect. D: Biol. Crystallogr.* **2010**, *66*, 213−221.
(39) Schomaker, V.; Trueblood, K. N. *Acta Crystallogr., Sect. B: Struct. Crystallogr. Cryst. Chem.* **1968**, *24*, 63−76.
(40) Chen, V. B.; Arendall, W. B.; Headd, J. J.; Keedy, D. A.; Immormino, R. M.; Kapral, G. J.; Murray, L. W.; Richardson, J. S.; Richardson, D. C. *Acta Crystallogr., Sect. D: Biol. Crystallogr.* **2010**, *66*, 12−21.
(41) Berman, H. M.; Westbrook, J.; Feng, Z.; Gilliland, G.; Bhat, T. N.; Weissig, H.; Shindyalov, I. N.; Bourne, P. E. *Nucleic Acids Res.* **2000**, *28*, 235−242.
(42) Zhang, Z.; Schäffer, A. A.; Miller, W.; Madden, T. L.; Lipman, D. J.; Koonin, E. V.; Altschul, S. F. *Nucleic Acids Res.* **1998**, *26*, 3986−3990.

DOI: 10.1021/acscatal.7b01854
ACS Catal. 2017, 7, 6877−6886